

Journal of Biomedical Optics

BiomedicalOptics.SPIEDigitalLibrary.org

Colposcopic imaging using visible-light optical coherence tomography

Lian Duan
Michael D. McRaven
Wenzhong Liu
Xiao Shu
Jianmin Hu
Cheng Sun
Ronald S. Veazey
Thomas J. Hope
Hao F. Zhang

SPIE.

Lian Duan, Michael D. McRaven, Wenzhong Liu, Xiao Shu, Jianmin Hu, Cheng Sun, Ronald S. Veazey, Thomas J. Hope, Hao F. Zhang, "Colposcopic imaging using visible-light optical coherence tomography," *J. Biomed. Opt.* **22**(5), 056003 (2017), doi: 10.1117/1.JBO.22.5.056003.

Colposcopic imaging using visible-light optical coherence tomography

Lian Duan,^a Michael D. McRaven,^b Wenzhong Liu,^a Xiao Shu,^a Jianmin Hu,^{a,c} Cheng Sun,^d Ronald S. Veazey,^e Thomas J. Hope,^b and Hao F. Zhang^{a,*}

^aNorthwestern University, Department of Biomedical Engineering, Evanston, Illinois, United States

^bNorthwestern University, Department of Cell and Molecular Biology, Chicago, Illinois, United States

^cWuhan University of Technology, School of Information Engineering, Wuhan, Hubei, China

^dNorthwestern University, Department of Mechanical Engineering, Evanston, Illinois, United States

^eTulane University, School of Medicine, Tulane National Primate Research Center, Covington, Louisiana, United States

Abstract. High-resolution colposcopic optical coherence tomography (OCT) provides key anatomical measures, such as thickness and minor traumatic injury of vaginal epithelium, of the female reproductive tract non-invasively. This information can be helpful in both fundamental investigations in animal models and disease screenings in humans. We present a fiber-based visible-light OCT and two probe designs for colposcopic application. One probe conducts circular scanning using a DC motor, and the other probe is capable of three-dimensional imaging over a $4.6 \times 4.6\text{-mm}^2$ area using a pair of galvo scanners. Using this colposcopic vis-OCT with both probes, we acquired high-resolution images from whole isolated macaque vaginal samples and identified biopsy lesions. © 2017 Society of Photo-Optical Instrumentation Engineers (SPIE) [DOI: 10.1117/1.JBO.22.5.056003]

Keywords: optical coherence tomography; colposcopy; optical biopsy; vaginal imaging.

Paper 170019RRR received Jan. 11, 2017; accepted for publication Apr. 17, 2017; published online May 8, 2017.

1 Introduction

Epithelium of the female reproductive tract (FRT) provides a natural and effective immunity against bacterial and viral antigens by not only acting as a physical barrier but also producing antimicrobial molecules, cytokines, and chemokines.¹ Epithelial disruption gives rise to various sexually transmitted infections (STI).² Thinning or loss of epithelial barrier is a risk factor for acquisition of human immunodeficiency virus (HIV).³⁻⁵ In recent years, concern has been raised that a microbicide, non-oxynol-9 (N-9), which was developed for contraception and STI prevention, may disrupt vaginal epithelium upon frequent use and even increase HIV transmission.⁶ Therefore, there is compelling demand for technologies to map vaginal epithelial morphology and provide measures of the FRT, which can be used for screening STI susceptible populations and evaluating vaginal products.

Currently, colposcopy is the standard technique for routine vaginal examination and safety assessment of vaginal products.² However, colposcopy can only detect severe epithelial pathological alterations, including focal bleeding, ulcers, peeling, and color variation. In addition, colposcopy itself only provides surface examination and cannot effectively measure the thinning of epithelial layers.^{4,6} Previous investigators relied on colposcopy-directed biopsy to obtain a cross-sectional view of the vaginal wall.⁷ Yet, biopsy is time-consuming and only can provide histology on a limited number of tissue sampling sites. More importantly, biopsy, as an invasive procedure, may damage the vaginal epithelium and increase the risk of STI.

Optical coherence tomography (OCT) is a well-established imaging modality that is capable of cross-sectional and three-

dimensional (3-D) imaging with microscale resolution.⁸⁻¹⁰ It can provide “optical biopsy” in human tissue noninvasively and has been applied to imaging the retina, skin, gastrointestinal tract, and other accessible anatomical sites.^{4,11-13} Fiber-based OCT is compact and portable^{14,15} and has been applied to colposcopic imaging previously.^{3,6} Vincent et al.⁴ detected N-9-induced vaginal epithelial thinning and injury in human subjects from OCT B-scans, which could not otherwise be identified by conventional colposcopy. More recently, Bell et al.¹⁶ applied fiber-based endoscopic OCT to safe assessment of vaginal microbicide, which involved measurement of epithelial and stromal thicknesses of mouse vagina.

Though vaginal epithelium examination and vaginal product evaluation by OCT are receiving increasing attention, previously reported colposcopic OCT suffered from a few limitations. First, the imaging systems only achieved moderate resolution. Both axial and lateral resolutions were tens of micrometers,^{3,4,6,16} which may not be ideal to resolve the mucosal and epithelial interface clearly and to evaluate epithelial integrity. Second, the imaging systems only provided cross-sectional B-scans of vaginal epithelial morphology. The 3-D imaging capability of OCT was not fully implemented.^{3,4,6,16}

In this work, we sought to overcome the limitations mentioned above and developed high-resolution 3-D OCT specifically for colposcopic applications. To gain high resolution, we switched to shorter wavelengths for illumination. Though conventional OCT uses near infrared (NIR) light source, recent technological advancement in supercontinuum lasers has facilitated the development of visible-light OCT (vis-OCT) for biomedical applications,¹⁷⁻¹⁹ which can achieve much higher resolution than NIR OCT with comparable spectral bandwidth.²⁰ In addition to higher resolution, vis-OCT may provide

*Address all correspondence to Hao F. Zhang, E-mail: hfzhang@northwestern.edu

better contrast. In biological tissue, the scattering coefficient often decreases with wavelength.²¹ Probing tissue with shorter wavelengths in OCT has the potential to improve imaging contrast from tissue whose scattering coefficient is low within the longer wavelength range. For example, the optical scattering coefficient in soft tissue at 560 nm is more than twice that at 860 nm.^{21,22} We previously demonstrated such contrast improvement in retinal imaging in both humans and rodents.^{19,20} Although using shorter wavelengths reduces OCT's penetration depth, it is still sufficient in colposcopic imaging when targeting the semitransparent mucus and mucosal-epithelium interface. Chen et al.²³ obtained images from *ex vivo* macaque vaginal tissue samples and measured the mucosal thickness using a free-space vis-OCT system, where the visible-light illumination offered clearly improved axial resolution as well as enhanced contrast between different tissues compared with OCT images obtained using NIR light.

We optimized OCT design specifically for colposcopic imaging. In general, design of endoscopic OCT is constrained by limited probe diameter (usually <1 mm) and the requirement of a flexible endoscopic probe. Most reported systems acquire two-dimensional (2-D) circular cross-sectional images using a DC motor, microelectro-mechanical system (MEMS), or fiber optic rotary joint.^{12,15,23-28} To achieve 3-D imaging, a pullback mechanism along the probe can be added either manually or mechanically.²⁹⁻³² In colposcopic imaging, however, the OCT probe does not require flexibility and only needs a relative short probe length (around 10 cm). In addition, a colposcopic OCT probe can be designed with a much larger diameter (several millimeters) as compared with vascular endoscopic OCT probes. Aimed at macaque vaginal lumen measurements, we determined our probe diameter to be 15 mm, which could flatten the folds on the vagina and make its surface attach to the probes with a moderate tension. The large size probe design follows the Cusco vaginal speculum (80 mm in length and 22 mm in width) and ultrasound colposcopic probe. In addition to meeting application requirements, this custom design brings several benefits compared with the conventional miniature design. First, we do not have to compromise the lateral resolution for a long depth of focus since the vaginal epithelium is closely attached to the glass window. Second, we can use standard achromatic lenses instead of gradient-index lenses, which are required for small-diameter probes but introduce severe chromatic aberration to broadband light illumination. Third, an external galvo-scanner pair can take the place of MEMS scanners that have usually been mounted in the probe for raster beam scanning in endoscopic OCT. While a MEMS scanner works at a certain resonant frequency and often requires high-voltage driving signals, the application of a galvo scanner brings improved scanning flexibility and reliability.^{33,34}

To fully implement local 3-D imaging while retaining a quick global inspection capability, we designed two colposcopic probes with different emphases. One probe realized circular scans with a DC motor for panoramic circular inspection of the vaginal wall, and the other was designed for 3-D imaging with a pair of galvo scanners for selected area examination. Using this colposcopic vis-OCT, we imaged the entire intact macaque vaginal vault. We compared OCT images with tissue histology and found good consistency. We demonstrated that colposcopic imaging by vis-OCT can measure vaginal epithelium thickness and detect minor disruptions in the vaginal wall.

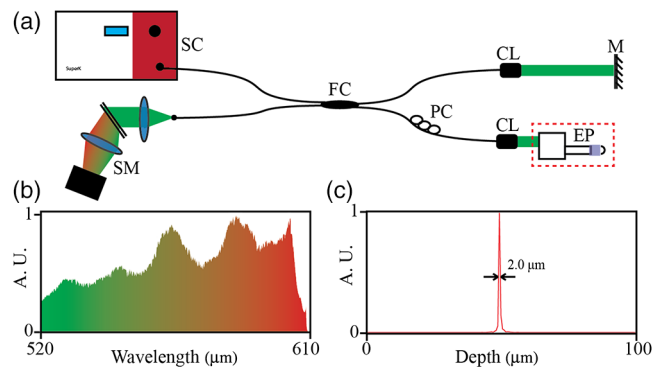


Fig. 1 Vis-OCT colposcopic imaging system. (a) Schematic of the fiber-based vis-OCT, (b) spectral envelope of the probe beam, (c) point spread function of a mirror signal measured in air. SC, supercontinuum source; FC, fiber coupler; CL, collimator; M, mirror; PC, polarization controller; EP, endoscopic probe; SM, spectrometer.

2 Experimental System

Figure 1(a) shows the schematic of the spectral-domain, fiber-based, endoscopic vis-OCT. We used a supercontinuum laser (SuperK EXTREME, NKT Photonics) as the light source. Long-pass (FF01-496/LP-25, Semrock) and short-pass (BSP01-633R-25, Semrock) filters filtered the probing beam with a central wavelength of 560 nm and a bandwidth of 90 nm. The spectral envelope is shown in Fig. 1(b). The system consisted of a fiber-based Michelson interferometer with a splitting ratio of 50/50. In the sample arm, the light was collimated by a collimator (HPUCO-23A-400/700-S-10AC, OZ Optics) and then propagated into the endoscopic probes for imaging. A polarization controller was added to the sample arm to balance the polarization states in the two arms. The combined light was spectrally dispersed by a transmission grating (1800 line/mm, Wasatch Photonics) and acquired by a line scan camera (spL4096-70km, Basler) with a 2048-pixel window. We imaged a mirror to obtain the spectral calibration and dispersion compensation data by analyzing the phases of the interference signals.³⁵ We quantified the axial resolution as the full-width-at-half-maximum value of the point-spread function as shown in Fig. 1(c). The axial resolution was measured to be 2.0 μm in air, which yielded an axial resolution of around 1.5 μm in biological tissue. We set the illumination power to 0.8 mW to minimize laser exposure while maintaining sufficient signal-to-noise ratio (SNR). We reduced the power to be lower than the previously reported values in NIR endoscopic OCT³⁶ to test whether an increased tissue scattering coefficient within the visible spectral range would provide an additional benefit. In future *in vivo* imaging experiments, we may adjust the illumination power within the laser safety limit to improve the SNR. The sensitivity of the system was characterized to be 89 dB, which was comparable with other vis-OCT systems using a supercontinuum light source and proved to be sufficient for both *in vivo* structural and functional imaging.^{19,20,37}

Figures 2(a) and 2(c) are, respectively, the schematics of the circular and raster scanning probes, and Figs. 2(b) and 2(d) are the photos of the two probes. Each probe body consisted of a rigid tube housing, a glass window tube, and a dome head. Both the rigid tube housing and the dome head were fabricated using a 3-D printer (Form 1+, Formlabs). We designed a slot in each of the rigid tube housings to precisely fix the focusing lens. The outer and inner diameters of the glass window tubes were

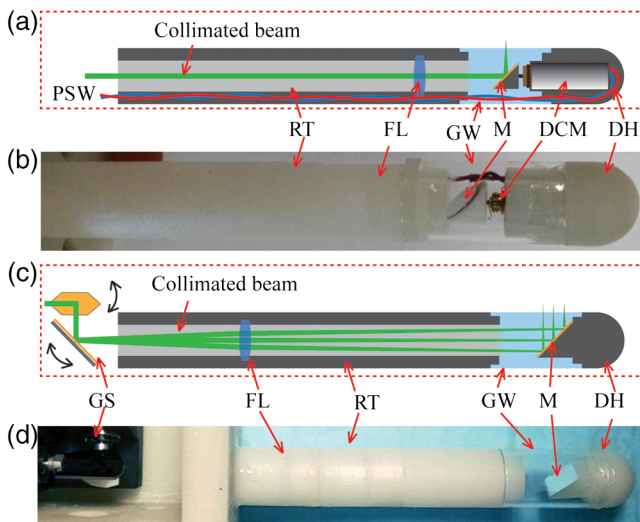


Fig. 2 Vis-OCT colposcopic imaging probes. (a) and (b) are the schematic and photograph of the circular scanning probe, respectively, (c) and (d) are the schematic and photograph of raster scanning probe, respectively. PSW, power supply wire; RT, rigid tube; FL, focus lens; GW, glass window; M, mirror; DCM, DC motor; DH, dome head; GS, galvo scanners.

15 and 13 mm, respectively. The lengths of the two tubes were around 110 mm. Each probe used a collimator with Ferrule Connector/Angled Physical Contact connector as the optical input so that we could conveniently switch probes.

In the circular scanning probe, we mounted a DC coreless motor at the distal end to deflect the beam. The collimated beam was focused by an antireflective-coated achromatic doublet lens (AC127-030-A-ML, Thorlabs). We fabricated a lightweight mirror by coating 100- μm aluminum onto the coverslip by an E-beam evaporator. We fixed the mirror on the motor with a 45-deg angle by lightweight mounts and index matching gel as shown in Figs. 2(a) and 2(b). The rotating speed of the motor was controlled by a variable voltage DC power supply. The circular scanning probe did not have mechanical pullback functionality and we manually translated the probe to image different circular B-scans. Each circular B-scan covered 47 mm corresponding to the circumference of the probe. The theoretical lateral resolution calculated based on optical design was 3.4 μm .

In the raster scanning probe, the collimated beam was scanned by a pair of galvo scanners and focused by an antireflective-coated achromatic doublet lens (AC127-075-A-ML, Thorlabs). A fixed 45 deg-oriented mirror reflected the beam onto the sample through the glass window. The maximum field of view was $5.6 \times 5.6 \text{ mm}^2$.

It has been previously reported that a glass window can act as a cylindrical lens in endoscopic OCT, which introduces astigmatism and degrades lateral resolution.^{38–40} In our probes, the large-diameter design made such effects minor. Since the diameters of the glass windows were much larger than their thickness and raster scanning range, the influence of the glass windows was approximately equivalent to a piece of flat glass. To verify this condition, we analyzed the astigmatism effect using ray tracing software (OpticStudioTM16, Zemax) and found that the change of focus spot radius caused by the glass window was $<1/10$ of the airy disk in both probes. This suggested that astigmatism caused by glass window tube was negligible. We also measured the lateral resolutions using a USAF resolution

target in directions along with and perpendicular to the axis of the raster scan probe. We found that the smallest resolvable bar patterns in both directions were in element 6 of group 5, which suggested a lateral resolution of 8.77 μm using the raster scan probe.

3 Experimental Results

We obtained female reproductive tissues of normal macaques from the Tulane National Primate Research Center. The samples were immersed in Roswell Park Memorial Institute medium and shipped refrigerated for overnight delivery. We dissected the FRT to obtain the whole intact vagina in phosphate-buffered saline solution at room temperature. A trained pathologist made a few biopsy cuts on the vaginal wall to landmark the sample for vis-OCT and histology imaging. Those cuts also induced lesions on the vaginal wall, which were imaged and identified in the experiments. All the samples were imaged within 24 h after collection, and all vis-OCT image acquisitions were completed within 2 h at room temperature. After imaging, we immediately trimmed the imaged areas into $5 \times 5 \text{ mm}^2$ pieces and kept them in aqueous gel. After freezing, samples were sent for histological analysis.

To acquire images, we gently inserted each probe into the entire intact vagina. The illuminating power was 0.8 mW. We first imaged the vaginal sample using the circular scanning probe. The camera integration time was 30 μs , and the DC motor rotating speed was 500 revolutions per minute, which generated a circular B-scan containing 4000 A-lines. We took 16 repeated circular B-scans during image acquisition, which could potentially be used to improve SNR through averaging. However, we did not perform averaging in Fig. 3 due to sufficiently high SNR. Figure 3(a) shows a full circle cross-sectional image of the macaque vagina acquired by the circular scanning probe. The image intensity is slightly higher from the 1 to 5 o'clock direction, but lower from the 6 to 9 o'clock direction, which is possibly caused by uneven illumination. The illumination optical path and focal distance could depend on the imaging angle if the rotating axis of the mirror was not well aligned with the probe axis. In addition, if the tissue was not tightly attached to the probe surface, the gap between them at certain scanning angles could also cause uneven intensity distribution of the detected OCT signals. Figures 3(b) and 3(c) are magnified views of the areas highlighted by the green and red regions in Fig. 3(a), respectively. The vertical black area in Fig. 3(b) was caused by the motor power supply wire blocking the beam. A hyporeflexive layer close to the surface (indicated by the yellow arrows) and an underlying hyperreflexive layer (indicated by the red arrows) can be clearly observed and differentiated in both Figs. 3(b) and 3(c). We correlated OCT images with histological results to verify the imaged anatomical structures by OCT. We used the biopsy cuts to locate the OCT scanned areas and took histology slides at the same locations. The observed structures in OCT images correlated well with the histology images as shown in Fig. 3(d), where the yellow and red arrows indicate the stratified squamous epithelium and underlying connective tissue, respectively.

We also imaged the vaginal sample using the raster scanning probe. We increased the camera integration time to 50 μs for better image quality. Figure 4(a) shows a B-scan image containing 1024 A-lines and covering a lateral length of 4.6 mm. The red dashed lines indicate the boundary between the epithelium and the connective tissue as observed from the histological slide

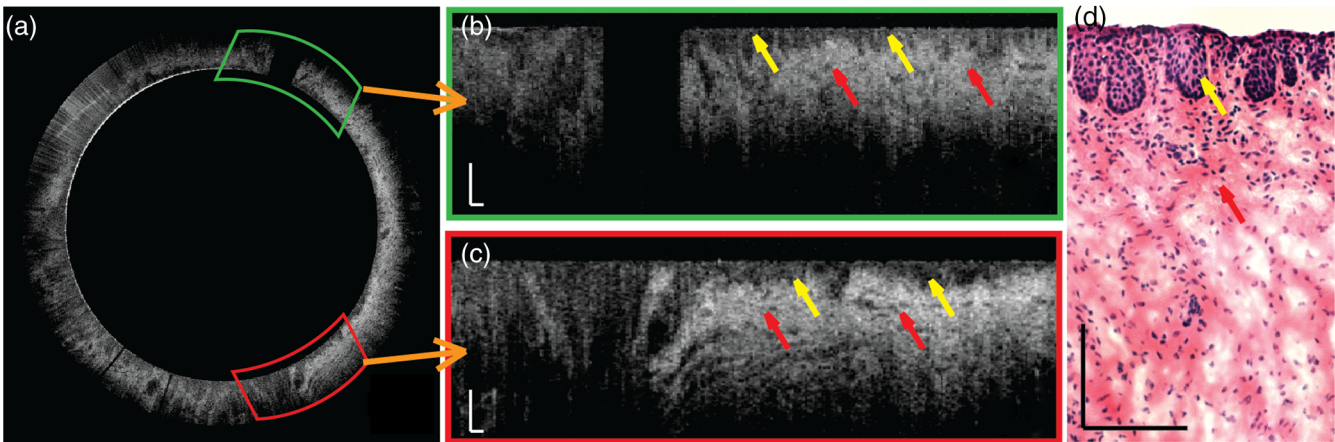


Fig. 3 Vis-OCT imaging using the circular scanning probe. (a) A typical circular B-scan image, (b) and (c) are magnified views of the highlighted areas in panel (a), (d) histology of normal macaque vaginal wall. Bars: 100 μm . Yellow and red arrows indicate epithelial layer and connective tissue, respectively.

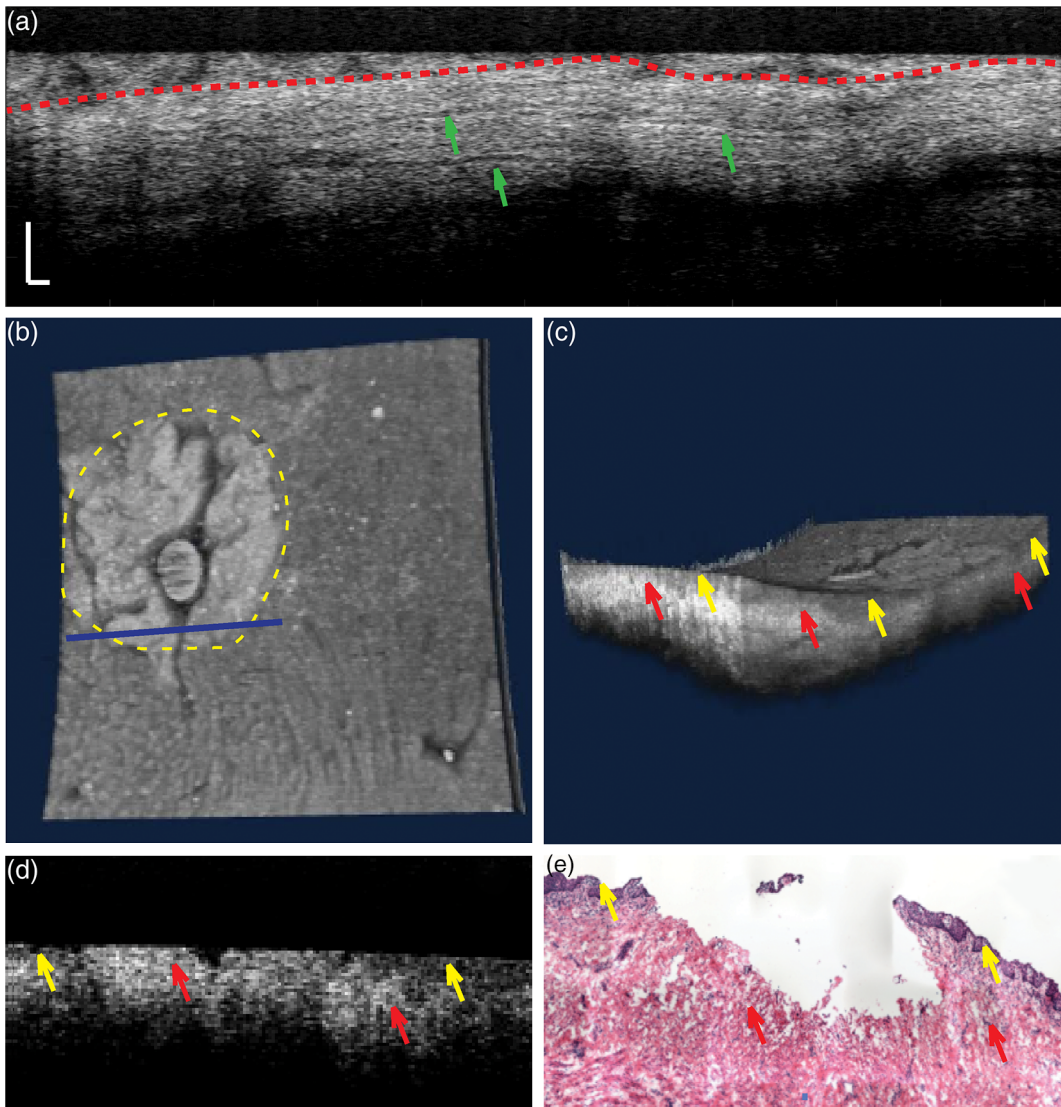


Fig. 4 Vis-OCT imaging using the raster scanning probe. (a) is a representative B-scan image; (b) and (c) are top and side views of 3-D-rendered vis-OCT dataset, (d) and (e) are cross-sectional OCT and histology images, respectively, of the tissue section from the position indicated by the blue line in panel (b). Green arrows indicate thin horizontal linear textures; yellow and red arrows indicate epithelial layer and connective tissue, respectively.

in Fig. 3(d). It is clear that the thickness of the epithelium layer varies at different lateral positions. The thickness changed from several micrometers to around 150 μm . In Fig. 4(a), we can observe several thin horizontal linear features as highlighted by the green arrows, which may be collagen bundles in the connective tissue.

The key strength of the raster scanning probe was to achieve 3-D imaging of the vaginal wall at selected areas with biopsy lesions. Figures 4(b) and 4(c) show a 3-D rendering of a volume dataset covering a biopsy cut in the vaginal wall. In this data set, 512×512 A-lines covered a 4.6×4.6 mm² area. Figure 4(b) is the top view of the volumetric rendering. The yellow dashed circle highlights the biopsy area, where the epithelium and a portion of the connective tissue were surgically removed. The area missing the epithelium is clearly visualized as a bright area on the surface of the rendering. From the side view shown in Fig. 4(c), the epithelium and connective tissue can be identified based on the intensity contrast in vis-OCT. Figures 4(d) and 4(e) show cross-sectional OCT and histological images of the biopsy cut from the location highlighted by the blue line in Fig. 4(b). We can observe that the epithelial layer was partially missing and the connective tissue is in direct contact with the endoscopic probe. It is clear that the hyperreflective layer (indicated by red arrows), which corresponds to the connective tissue, appeared on the surface of the tissue.

4 Discussion and Conclusion

In this work, we developed the first fiber-based vis-OCT system for colposcopic imaging and used it to image macaque vaginal tracts. This colposcopic imaging system combined improved resolution and higher imaging contrast of vis-OCT (as compared with OCTs using NIR light). To meet different imaging needs, we developed a circular scanning probe with a DC motor and a raster scanning probe with a pair of galvo scanners. The circular scanning probe first provided panoramic cross-sectional circular views of the vaginal track and helped to quickly identify the region of interest (ROI), such as biopsy lesions or potentially epithelial disruption. The raster scanning probe then generated 3-D imaging of the ROI with higher sampling density and scanning flexibility. The two probes were complementary to each other and were designed for easy switching. One technological limitation in the current design was the lack of pullback functionality for the circular scanning probe, which, therefore, could only provide 2-D imaging on itself. In the future, the two probes can potentially be integrated.

As the next step, we intend to use this vis-OCT colposcopic imaging system for vaginal examination in primates *in vivo*, which will set the stage for human tests. As revealed in recent studies, foci of impaired barrier function and inflammation may be portals for STI.^{41,42} However, local sampling methods, such as lavages and biopsies, may not be able to adequately evaluate these processes. The high-resolution images shown in this work demonstrated that vis-OCT can successfully identify both the epithelium and the connective layers, map the thickness of the epithelial layer, detect biopsy lesions, and potentially identify minor disruptions within the vaginal epithelium. Therefore, our vis-OCT colposcopic imaging system has the potential to characterize vaginal epithelial barriers and evaluate the safety of vaginal products, such as microbicide.

Due to the relatively large diameter of our probes, we were unable to image the canal of the endocervix. A smaller outer diameter is required to access the endocervical canal for

examination. Using a fiber connection, a new probe can be readily adapted to our fiber-based vis-OCT system. Based on future *in vivo* test, we may modify our probes to conduct endocervical imaging in primates. In addition to ultrahigh-resolution morphology, we will also explore the possibilities to quantify hemodynamics-related parameters using our vis-OCT colposcopic imaging.^{17,30,37,43}

Disclosures

Hao F. Zhang, Cheng Sun, and Wenzhong Liu have financial interests in Opticent Health, which, however, did not support this work.

Acknowledgments

We greatly appreciate technical assistance from Dr. Hao Li, Dr. Biqin Dong, and Meagan Watkins. We also acknowledge generous financial support from the National Institutes of Health (NIH) grants R01AI094595, R33AI094584, R24EY022883, and DP3DK108248 and a pilot grant from the Third Coast Center for AIDS Research as part of NIH P30AI117943.

References

1. C. R. Wira, K. S. Grant-Tschudy, and M. A. Crane-Godreau, "Epithelial cells in the female reproductive tract: a central role as sentinels of immune protection," *Am. J. Reprod. Immunol.* **53**, 65–76 (2005).
2. W. H. Organization, *Manual for the Standardization of Colposcopy for the Evaluation of Vaginal Products*, World Health Organization, Geneva (2004).
3. K. L. Vincent et al., "High resolution imaging of epithelial injury in the sheep cervicovaginal tract: a promising model for testing safety of candidate microbicides," *Sex. Transm. Dis.* **36**, 312–318 (2009).
4. K. L. Vincent et al., "Optical coherence tomography compared with colposcopy for assessment of vaginal epithelial damage: a randomized controlled trial," *Obstet. Gynecol.* **118**, 1354–1361 (2011).
5. R. J. Shattock and J. P. Moore, "Inhibiting sexual transmission of HIV-1 infection," *Nat. Rev. Microbiol.* **1**, 25–34 (2003).
6. K. L. Vincent et al., "Application of optical coherence tomography for monitoring changes in cervicovaginal epithelial morphology in macaques: potential for assessment of microbicide safety," *Sex. Transm. Dis.* **35**, 269–275 (2008).
7. D. L. Patton et al., "Epithelial cell layer thickness and immune cell populations in the normal human vagina at different stages of the menstrual cycle," *Am. J. Obstet. Gynecol.* **183**, 967–973 (2000).
8. D. Huang et al., "Optical coherence tomography," *Science* **254**, 1178–1181 (1991).
9. A. M. Zysk et al., "Optical coherence tomography: a review of clinical development from bench to bedside," *J. Biomed. Opt.* **12**, 051403 (2007).
10. W. Drexler and J. G. Fujimoto, Eds., "Optical coherence tomography: technology and applications," in *Biological and Medical Physics, Biomedical Engineering*, p. 1346, Springer-Verlag Berlin Heidelberg, Heidelberg, Germany (2008).
11. J. G. Fujimoto et al., "Optical biopsy and imaging using optical coherence tomography," *Nat. Med.* **1**, 970–972 (1995).
12. G. J. Tearney et al., "In vivo endoscopic optical biopsy with optical coherence tomography," *Science* **276**, 2037–2039 (1997).
13. R. John et al., "Three-dimensional optical coherence tomography for optical biopsy of lymph nodes and assessment of metastatic disease," *Ann. Surg. Oncol.* **20**, 3685–3693 (2013).
14. B. H. Lee, E. J. Min, and Y. H. Kim, "Fiber-based optical coherence tomography for biomedical imaging, sensing, and precision measurements," *Opt. Fiber Technol.* **19**, 729–740 (2013).
15. C. Zhou et al., "Endoscopic optical coherence tomography," *Optical Coherence Tomography: Technology and Applications*, pp. 2077–2108, Springer International Publishing, Switzerland (2015).

16. B. A. Bell et al., "Optical coherence tomography for assessment of microbicide safety in a small animal model," *J. Biomed. Opt.* **18**, 046010 (2013).
17. J. Yi et al., "Visible light optical coherence tomography measures retinal oxygen metabolic response to systemic oxygenation," *Light Sci. Appl.* **4**, e334 (2015).
18. S. P. Chong et al., "Quantitative microvascular hemoglobin mapping using visible light spectroscopic optical coherence tomography," *Biomed. Opt. Express* **6**, 1429–1450 (2015).
19. J. Yi et al., "Human retinal imaging using visible-light optical coherence tomography guided by scanning laser ophthalmoscopy," *Biomed. Opt. Express* **6**, 3701–3713 (2015).
20. S. Chen et al., "Dual-band optical coherence tomography using a single supercontinuum laser source," *J. Biomed. Opt.* **21**, 066013 (2016).
21. S. L. Jacques, "Optical properties of biological tissues: a review," *Phys. Med. Biol.* **58**, R37 (2013).
22. J. M. Schmitt and G. Kumar, "Optical scattering properties of soft tissue: a discrete particle model," *Appl. Opt.* **37**, 2788–2797 (1998).
23. S. Chen et al., "Imaging endocervical mucus anatomy and dynamics in macaque female reproductive track using optical coherence tomography," *Quantum Imaging Med. Surg.* **5**, 40–45 (2014).
24. W. Jung et al., "Three-dimensional endoscopic optical coherence tomography by use of a two-axis microelectromechanical scanning mirror," *Appl. Phys. Lett.* **88**, 163901 (2006).
25. D. C. Adler et al., "Three-dimensional endomicroscopy using optical coherence tomography," *Nat. Photonics* **1**, 709–716 (2007).
26. Z. G. Wang et al., "In vivo bladder imaging with microelectromechanical systems-based endoscopic spectral domain optical coherence tomography," *J. Biomed. Opt.* **12**, 034009 (2007).
27. D. C. Adler et al., "In vivo endomicroscopy using three-dimensional optical coherence tomography and Fourier domain mode locked lasers," *Proc. SPIE* **6847**, 684708 (2008).
28. N. Zhang et al., "Compact piezoelectric transducer fiber scanning probe for optical coherence tomography," *Opt. Lett.* **39**, 186–188 (2014).
29. D. C. Adams et al., "Advances in endoscopic optical coherence tomography catheter designs," *IEEE J. Sel. Top. Quantum Electron.* **22**, 210–221 (2016).
30. H.-C. Lee et al., "Su1715 ultrahigh speed endoscopic optical coherence tomography angiography for visualization of subsurface vasculature in Barrett's esophagus and dysplasia," *Gastrointest. Endosc.* **81**, AB388 (2015).
31. H. Pahlevaninezhad et al., "An endoscopic imaging system for co-registered Doppler optical coherence tomography and autofluorescence imaging of human airways in vivo," in *Optics in the Life Sciences, OSA Technical Digest (online)*, Optical Society of America, BM4A.4 (2015).
32. T.-H. Tsai et al., "Ultrahigh speed endoscopic optical coherence tomography for gastroenterology," *Biomed. Opt. Express* **5**, 4387–4404 (2014).
33. K. H. Kim et al., "Two-axis magnetically-driven MEMS scanning catheter for endoscopic high-speed optical coherence tomography," *Opt. Express* **15**, 18130–18140 (2007).
34. C. D. Lu et al., "Handheld ultrahigh speed swept source optical coherence tomography instrument using a MEMS scanning mirror," *Biomed. Opt. Express* **5**, 293–311 (2014).
35. L. Duan, T. Marvdashti, and A. K. Ellerbee, "Polarization-sensitive interleaved optical coherence tomography," *Opt. Express* **23**, 13693–13703 (2015).
36. W. Yuan et al., "Optimal operational conditions for supercontinuum-based ultrahigh-resolution endoscopic OCT imaging," *Opt. Lett.* **41**, 250–253 (2016).
37. S. Chen et al., "Retinal oximetry in humans using visible-light optical coherence tomography [Invited]," *Biomed. Opt. Express* **8**, 1415–1429 (2017).
38. J. F. Xi et al., "High-resolution OCT balloon imaging catheter with astigmatism correction," *Opt. Lett.* **34**, 1943–1945 (2009).
39. D. Lorensen et al., "Ultrathin side-viewing needle probe for optical coherence tomography," *Opt. Lett.* **36**, 3894–3896 (2011).
40. P. Meemon et al., "Optical design of a dynamic focus catheter for high-resolution endoscopic optical coherence tomography," *Appl. Opt.* **47**, 2452–2457 (2008).
41. R. F. Baggaley, R. G. White, and M.-C. Boily, "HIV transmission risk through anal intercourse: systematic review, meta-analysis and implications for HIV prevention," *Int. J. Epidemiol.* **39**(4), 1048–1063 (2010).
42. M. Stockmann et al., "Mechanisms of epithelial barrier impairment in HIV infection," *Ann. N.Y. Acad. Sci.* **915**, 293–303 (2000).
43. W. A. Welge and J. K. Barton, "In vivo endoscopic Doppler optical coherence tomography imaging of mouse colon," *Proc. SPIE* **9691**, 96910T (2016).

Biographies for the authors are not available.